Available online at www.sciencedirect.com

SciVerse ScienceDirect

Journal of the European Ceramic Society 32 (2012) 1593–1603

www.elsevier.com/locate/jeurceramsoc

# Bulk composition and microstructure dependence of effective thermal conductivity of porous inorganic polymer cements

E. Kamseu [a,*], B. Nait-Ali [b], M.C. Bignozzi [c], C. Leonelli [a], S. Rossignol [b], D.S. Smith [b]

[a] Department of Materials and Environmental Engineering, University of Modena and Reggio Emilia, Via Vignolese 905, 41125 Modena, Italy
[b] Groupe d'Etude des Matériaux Hétérogènes, Centre Européen de la Céramique, 12 rue Atlantis, 87068 Limoges Cedex, France
[c] Department of Civil, Environmental and Materials Engineering, University of Bologna, Via Terracini 28, 40131 Bologna, Italy

Received 7 July 2011; received in revised form 11 November 2011; accepted 28 December 2011
Available online 29 January 2012

**Abstract**

Experimental results and theoretical models are used to assess the effective thermal conductivity of porous inorganic polymer cements, often indicated as geopolymers, with porosity between 30 and 70 vol.%. It is shown that the bulk chemical composition affects the microstructure (grains size, pores size, spatial arrangement of pores, homogeneity, micro cracks, bleeding channels) with consequently the heat flow behaviour through the porous matrix. In particular, introduction of controlled fine pores in a homogeneous matrix of inorganic polymer cements results in an increase of pore volume and improvement of the thermal insulation. The variation of the effective thermal conductivity with the total porosity was found to be consistent with analytical models described by Maxwell–Eucken and Landauer.


*Keywords:* Thermal conductivity; Porosity; Inorganic polymer cements; Microstructure-final; Composites

## 1. Introduction

The porous and amorphous structure of inorganic polymer cements (IPC), often indicated as geopolymers, implies that flow in a thermal gradient will take a very tortuous route consisting of a multiple of neighboring interconnected polysialate particles.[1] The effective thermal conductivity of such a material is strongly affected by its chemical composition as well as the presence of voids in the microstructure which are pockets or cells more or less spherical in shape.[2] The microstructure of IPC is known to vary considerably with chemical composition and processing conditions. For example, related to the preparation, a controlled fine porosity can be incorporated into the skeletal framework, which also reduces the effective density of gel. In particular for geopolymers, it has been demonstrated that the pore size varies with Si/Al ratio. The porosity includes interconnected pores ranging from nano to micrometric scale (10–50 nm for Si/Al molar ratio ~1, <10 nm for Si/Al molar ratio ~1.65 and very fine pores (~5 nm) for Si/Al molar ratio ~2.5.[3,4] Apart from these fine pores, some dispersed larger-diameter pores are generally observed which can be controlled during processing. The pore structure is determined by the nature and size of polysialates formed as well as by the interactions between various phases present in the material.[4–6] The distribution and interconnectivity of pores, the short-range ordering of the gel phase, and the nominal composition are all likely to play roles in determining the heat transport properties of geopolymeric gels.[1,7] In particular the effective thermal conductivity of IPC will be controlled by the pore size distribution and pore volume.

In this work, we exploit the corrosion of aluminum powder in a highly concentrated alkali solution to form porous IPC. Normal processing of geopolymer material leads to a pore fraction of 25–30% of total porosity.[1,8] Upon introduction of a foaming agent into the geopolymer paste, the resultant steam forms bubbles within the softened matrix to produce a frothy-like structure which transforms into a cellular material. The additional pores increase the pore volume fraction up to 70%.

Previous investigations on compositions of geopolymer materials already were devoted to their suitability as structural materials.[8] In the case of the more porous materials which were obtained, first measurements indicated their potential for thermal insulation.[1] Here we investigate the relations between the bulk composition, the pore size-distribution, pore volume fraction and the effective thermal conductivity of the porous geopolymer.

* Corresponding author.
*E-mail address:* Kamseuelie2001@yahoo.fr (E. Kamseu).

0955-2219/$ – see front matter © 2012 Elsevier Ltd. All rights reserved.
doi:10.1016/j.jeurceramsoc.2011.12.030

**Nomenclature**

| | |
|---|---|
| $\lambda_{eff}$ | effective thermal conductivity |
| $\lambda_s$ | thermal conductivity of solid continuous phase |
| $\lambda_g$ | thermal conductivity of dispersed phase (air) |
| $v_s$ | volume of solid fraction |
| $v_g$ | volume of dispersed phase |
| $F$ | form factor regarding the pores |
| $v_p$ | volume of pores |
| $\cos^2 \alpha$ | orientation parameter |
| HB | high bound or upper bound of Hashin–Shtrikman |
| LB | lower bound of Hashin–Shtrikman |
| $a$ and $b$ | calibration curve constants |
| $\Delta T$ | difference of temperature |
| $R$ | thermal resistance |
| $\phi$ | heat flux density |
| $U$ | thermo electric power |
| $r$ | pore radius |
| $\gamma$ | surface tension of mercury |
| $\theta$ | contact angle |

## 2. Analytical models for the effective thermal conductivity of porous geopolymers

A significant number of analytical models have been developed to predict the effective thermal conductivity of porous solid as function of pore volume fraction. They differ in the manner by which the morphology of the pore system has been taken into account. In this respect Collishaw and Evans have written a useful review.[9]

As reported in our previous work[8] and by many other authors,[3–6] the metakaolin based geopolymer is typically made of nanometric scale particles of polysialates joined to one another to form a matrix containing nanosized pores. Furthermore, a small fraction of porosity is micrometric, and micro cracks are also visible. Therefore, an analytical model yielding on equation that can be used to describe satisfactorily the effective thermal conductivity of a porous geopolymer material is difficult to identify. However in the respect we consider a matrix of porous geopolymer to be constituted of particles, cement (binding the particles of polysialates and other residues together), air inside pores and finally micro cracks. The material can be classified as bound/cemented matrix.[9] In addition, secondary effects influencing the effective thermal conductivity may include contact resistance between grains, radiation through grains or pores, convection and in the case of small pores, the Knudsen effect which can reduce the gas thermal conductivity.[9]

Studies of the effect of structure on the heat flow and effective thermal conductivity ($\lambda_{eff}$) have shown that $\lambda_{eff}$ is generally higher in cemented materials.[10–12] Thus the increase in porosity for geopolymer matrices is a potential solution to maintain the strength while improving the insulating behaviour of the materials. A porous geopolymer is then considered as a continuous solid phase in which uniformly dispersed cavities are filled with fluid (air, or another gas). An approach describing this type of solid phase has been proposed by Hashin–Shtrikman.[2] The approach is based on calculating the most restrictive bounds for the value of the effective thermal conductivity. The primary parameters influencing the effective thermal conductivity are the conductivity ratio and concentration of voids. The upper bound (HB) refers to a continuous solid phase including uniformly dispersed fluid filled cavities (Eq. (1)).

$$\lambda_{eff} = \lambda_s + \frac{3p\lambda_s(\lambda_g - \lambda_s)}{3\lambda_s + (1-p)(\lambda_g - \lambda_s)} \quad (1)$$

And the lower bound (LB) refers to a continuous fluid phase including uniformly dispersed solid spheres (Eq. (2)).

$$\lambda_{eff} = \lambda_g + \frac{3\lambda_g(1-p)(\lambda_s - \lambda_g)}{3\lambda_g + p(\lambda_s - \lambda_g)} \quad (2)$$

Maxwell–Eucken[13] model can also be used as $\lambda_s$ is the thermal conductivity of the continuous phase and $\lambda_g$ that of the dispersed phase (air or hair saturated humidity in IPC voids). The Maxwell–Eucken model considers a random distribution of pores with different diameters (Eq. (3)).

$$\lambda_{eff} = \frac{\lambda_s v_s + \lambda_g v_g((3\lambda_s)/(2\lambda_s + \lambda_g))}{v_s + v_g((3\lambda_s)/(2\lambda_s + \lambda_g))} \quad (3)$$

In fact the Maxwell–Eucken equation (3) leads to an expression arithmetically equivalent to Eq (1).

Broadbent and Hammersley[14] studied situations of fluid flow through a porous medium where percolation becomes important. The hypothetical passage of a fluid through an uncertain porous environment. For a metallic phase randomly introduced in an insulator to form a composite, the composite behaves like an insulator in the case of a weak concentration of the metallic phase. If the volume fraction of metal increases, the current can circulate between two opposite faces of the material via the metallic phase and the composite behaves like a conductor. The volume fraction at which this change of behaviour is observed is called the percolation threshold. This can be illustrated by Landauer's expression for the effective thermal conductivity of a mixture of two phases with each phase constituted of particle sizes of roughly equivalent size[15] (Eq. (4)):

$$\lambda_{eff} = \frac{1}{4}[\lambda_g(3v_g - 1) + \lambda_s(3v_s - 1) + ([\lambda_g(3v_g - 1) + \lambda_s(3v_s - 1)]^2 + 8\lambda_s\lambda_g)^{1/2}] \quad (4)$$

The percolation model[15] assumes a completely random distribution of these components, and is equivalent to an Effective Medium Theory (EMT)[16,17] (Eq. (5)).

$$v_s\frac{\lambda_s - \lambda_{eff}}{\lambda_s + 2\lambda_{eff}} + v_g\frac{\lambda_g - \lambda_{eff}}{\lambda_g + 2\lambda_{eff}} = 0 \quad (5)$$

Nait-Ali et al.[18] have demonstrated the close agreement between predicted values of the effective thermal conductivity using Eq. (4) and experimental values for zirconia with pore volume fraction up to 70%.

In this manuscript, the thermal characterization of porous geopolymer materials is presented. First synthesis and characterization of the porous geopolymers are described. Then, the experimental setup and associated analysis for measuring the thermal conductivity of the synthesized materials are presented. Finally the thermal conductivity of porous geopolymers is discussed in regard to the most suitable models available in the literature for the effective thermal conductivity of the cemented porous matrices. Experimental results are compared to predictions by Maxwell–Eucken which is equivalent to Hashin and Shtrikman (upper bound) and Landauer's expression (percolation).

## 3. Experimental methods

### 3.1. Materials and preparation of porous geopolymers

Two different aluminosilicate (metakaolin) powders were prepared by firing at 700 °C for 4 h; a standard kaolin and the other rich in sand.[1] The two materials were ground finely to a particle size <80 μm. The Brunauer–Emmett–Teller (BET) surface areas of the aluminosilicates, as determined by nitrogen adsorption with a micrometrics GEMINI 2360 instrument are 17.10 and 24.32 $m^2/g$ respectively for the standard and the sand-rich compositions of metakaolin. Alkaline solution was prepared by mixing the sodium/potassium hydroxide (reagent grade, Carlo Erba, Italy) solution (7.5 M) with sodium silicate, $SiO_2/Na_2O = 3$ and L.O.I = 40 wt%, 1:1:2 volume ratio.

To prepare porous geopolymers, 5 different compositions of metakaolin were tested, each with a specific Si/Al molar ratio. This was achieved by mixing different proportions of the standard and sand-rich aluminosilicates. Alkaline solution was added to each powder with a solid/liquid ratio of 1.66. Finally the formulations denoted IPM, IP75M, IPMT, IP25M and IPT were obtained with respective Si/Al molar ratios of 1.23, 1.50, 1.79, 2.0 and 2.42. For all the five formulations, the Na/Al ratio was close to 1 to achieve homogeneous slurry and balance the negative charge of alumina oligomers. The pastes were mechanically mixed in a ball-mill for 10 min and then the pore forming agent (prepared from metallic powder, in a very low concentration to avoid influence on the bulk composition of the geopolymer) was added at different concentrations C0, C1, C2, C3 and C4. C0 did not contain any addition of aluminum powder. C1, C2, C3 and C4 correspond to 5, 10, 15 and 20 mg of metallic powder for 100 ml of alkaline solution respectively. C4 produced about 70 vol.% of porosity (IPMT, IP25M and IPT) and constitutes the upper limit at which solid skeleton in these porous geopolymers was geometrically describable. For samples with low Si/Al molar ratio (IPM and IP75M), the pore volume fraction was in the range 65–70% with concentration C3. After the addition of the foaming agent continuous mixing was made for 5 min before the slurries were transferred into Teflon® molds to prepare prisms of 30 mm × 30 mm and cylinders with 18.85 mm in diameter. The thickness of prisms varies from 1.5 to 6 mm and that of cylinders varies from 1 to 3 mm. The samples were cured in sealed plastic for two weeks in air so that constant weight could be achieved. The samples were then polished to insure the planarity and regularity. The porosity was evaluated in terms of volume fraction and size distribution before the thermo physical characterization.

### 3.2. Mercury intrusion porosimeter and microtomography

A mercury-intrusion type porosimeter (MIP, Carlo Erba 2000) equipped with a macropore unit (Model 120, Fison Instrument) was used to measure the pores with size <20 μm. The geopolymer specimens were crushed to particles of approximately 8–10 mm across (volume ~1 $cm^3$). The measurements were performed with a maximum applied pressure of 2000 bar for pore size in the range between 0.004 and 20 μm. Pore size radius ($r$) was calculated by Washburn's equation, assuming a contact angle ($\theta$) of 141.3° and a Hg surface tension ($\gamma$) of 480 dyn/cm:

$$r = -\frac{2\gamma\cos\theta}{p} \quad (6)$$

where $p$ is the intrusion pressure. The input data of pressure, intruded mercury volume, sample mass, and sample volume (determined by pycnometry) are needed to calculate the pore-size distribution, the cumulative pore volume at maximum or defined pressure and characteristics such as the average pore radius, the bulk density and the apparent density.

It should be noted while that some parameters such as moisture content, theoretical assumptions and inaccuracies in the data evaluation (e.g.: only pore neck size is really measured, calculation with an assumed constant value for the contact angle) can affect the accuracy of measurements.[19–22] However, unlike the enduring scientific discussions whether mercury-intrusion porosimetry is an appropriate method to estimate pore-size distribution of structural materials, a proper care during sample preparation allows the method to review pore-size distribution curves and modifications of the pore structure of a material qualitatively.[22–26]

For pores ≥20 μm, computerized micro tomography (μCT) measurements were made, using a Skyscan 1172, (Skyscan B.V., Leuven, Belgium), at 80 kV with 100 μA, with no additional filtering and an image pixel size of 10.1 μm. Cell and strut size were evaluated with a CT-Analyzer (CTan), 1.10.0, (Skyscan B.V., Leuven, Belgium), on a minimum of 250 slices for each sample. Visualization of the scanned images was performed using Amira 5.3.2 software (Visage Imaging GmbH, Berlin, Germany) with Voltex displaying mode. Scanning and reconstruction time was 90 min for each sample on a quad core E9500 PC with 8GB RAM. The 3D evaluation took between 1 h and 4 h per sample depending on the pore volume fraction with a total amount of 60 GB data.

The MIP and micro tomography techniques were used to calculate the total porosity of the porous geopolymer specimens. The results obtained through these two methods were validated with those obtained using the density of the specimens (determined with a density analyser instrument GEOPYC 1360 type Micromeritics) and that obtained with a mercury pycnometer. The two values permitted to determine the pore volume

fraction. The instrument gives result of five measurements for each specimen. The measurements were performed on the samples after 24 h in the oven at 110 °C.

### 3.3. Thermal conductivity measurement

#### 3.3.1. Thermal conductivity

*3.3.1.1. Heat flux meter method 1.* The determination of the effective thermal conductivity using the Heat Flow Meter (ASTM C518, ISO8301) requires homogeneous samples with parallel flat faces. The apparatus is based on the application of Fourier's law in steady state conditions. A thermal gradient is imposed across the sample which is maintained between two copper plates, the upper is used as a heat source. The difference in temperature between the two copper plates ($\Delta T$) and the heat flux density ($\phi$) are obtained with convenient sensors. The apparent thermal resistance ($R$) is then calculated as:

$$R = \frac{\Delta T}{\phi} \tag{7}$$

The procedure is based on multi thicknesses of the sample. Thermal contact resistances (or contact resistivity) may cause huge errors of thermal conductivity measurements if it is not taken into account. The sample's thermal resistance $R_{\text{sample}}$ is equal to the sample's thickness $x$ (m) divided by its thermal conductivity $\lambda$ ($m^2\,K^{-1}\,W^{-1}$).

$$R_{\text{sample}} = \frac{x}{\lambda} \tag{8}$$

Thermal contact resistance ($R_{\text{contact}}$) depends on the material, its roughness, and the interface pressure. It is equal to temperature difference between the two contacting surfaces $\delta T$ divided by heat flux $q$ ($W\,m^{-2}$).

$$R_{\text{contact}} = \frac{\delta T}{q} \tag{9}$$

The apparent thermal resistance of the sample placed into the instrument is the sum of these contributions and equal to:

$$R_{\text{total}} = \frac{x}{\lambda} + 2R_{\text{contact}} \tag{10}$$

The total resistance is proportional to the heat flux $q$ across the sample which is a function of the temperature difference $\Delta T$ between instrument's plates and inversely proportional to the total resistance $R_{\text{total}}$ ($W\,m^{-2}$):

$$q = SQ = \frac{\Delta T}{R_{\text{total}}} = \Delta T\left(\frac{x}{\lambda} + 2R_{\text{contact}}\right) \tag{11}$$

In the case of thermally insulating materials (small $\lambda$) the sample's thermal resistance is large and the thermal contact resistance can be neglected. Plotting the graph of the thermal resistance as function of thickness and extrapolation down to zero thickness gives the value of thermal contact resistance of the two surfaces ($2R_{\text{contact}}$). The reciprocal of the slope ($\Delta x/\Delta R_{\text{total}}$) is equal to the correct effective thermal conductivity of the material:

$$\lambda = \frac{x_2 - x_1}{x_2/\lambda + 2R_{\text{contact}} - x_1/\lambda - 2R_{\text{contact}}} \tag{12}$$

where $x_1$ and $x_2$ are thickness of the thin and thick samples. Multi-thickness give better accuracy. The apparent thermal contact resistance is assumed not to vary following polishing. For this study, we used square samples 30 mm × 30 mm with various thicknesses in the range 1.5–6 mm. The polished samples were cleaned with compressed air to remove powder residues from the pores.

*3.3.1.2. Heat flux meter method 2.* The thermal conductivity of the porous bodies was measured on disk samples of a diameter 18.85 mm and thickness between 1 and 3 mm using a self-made apparatus constructed according to DIN51908 with a brass as reference body. A calibration curve relating the thermoelectric power $U$ with the thermal conductivity was constructed and the data was fitted by the least squares method. From the calibration curve, the constants $a$ and $b$ were computed (1.89 and 2.68 respectively) and used to determine the thermal conductivity of porous samples as according to Eq. (13):

$$U = \frac{a}{(b/(\lambda/l)) + 1} \tag{13}$$

where $\lambda$ is the thermal conductivity of the sample and $l$ the thickness.

### 3.4. Experimental characterization of microstructure: ESEM

The Environment Scanning Electron Microscopy (ESEM) technique was used to determine the 2D morphological features of the fresh fractured pieces of porous geopolymers. For the fractured specimens, the anhydrous phases of the geopolymers appear light to dark gray. The pores, being absence of solid, do not scatter electrons and appear uniformly black. In order to allow comparison, the technical parameters were constant for all the samples. ESEM was used essentially for the characterization of the macro pores. Micrographs were obtained at different magnification from 5000× to 50×. The fine pores were investigated using the MIP (Mercury Intrusion Porosimeter) and micro tomography.

### 3.5. Water charging and decharging capacity of porous geopolymer materials

Exposition at ambient temperature and weight variation measurements at temperatures between 20 °C and 100 °C were used to investigate the capacity of the insulating materials to accumulate and lose humidity. The samples were first cured up to a constant weight in laboratory (20 ± 5 °C and ∼55% of relative humidity). The samples were then placed in the oven at 100 °C for 24 h. The total weight loss measured just after removal was used to calculate the saturation in humidity ($T$). Then the weight gained progressively ($T_x$) was measured as function of time.

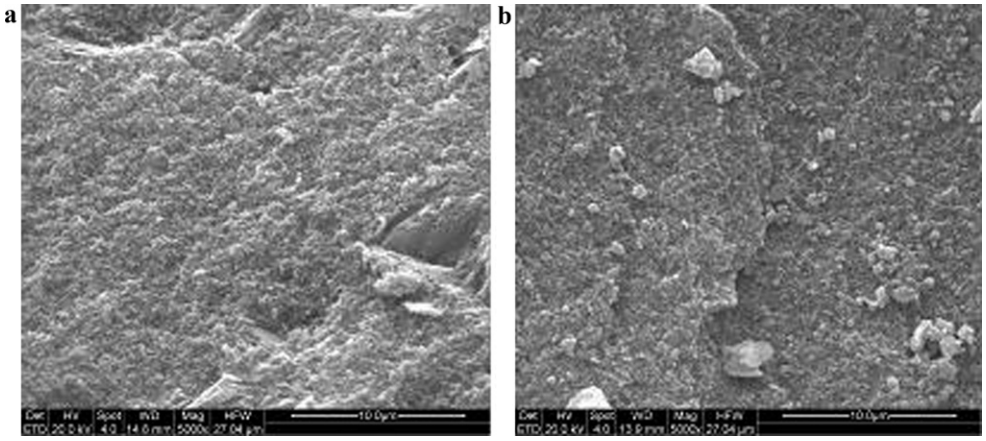


Fig. 1. Micrographs of fresh fractured matrix of dense geopolymer: (a) Si/Al <1.79 and (b) Si/Al >1.79.

## 4. Results

### 4.1. Microstructure and porosity

Fig. 1 shows the micrographs of: (a) the geopolymer matrix with low Si/Al (1.23, 1.50, 1.79) and (b) the geopolymer matrix with a relatively high Si/Al (2.0, 2.42). The two micrographs are dominated by H–M–A–S gel which consists of colloidalized globular units of diameter <1 μm closely bonded together. At high magnification their amorphous nature is well pronounced[8] with fine porosity. The micrograph 1b is relatively coarse microstructure when compared to samples reported in Fig. 1a: numerous and roughly similar-sized globular units are observed. The difference is related to the size of H–M–A–S formed during the geopolymerization and the presence of non-reacted residues of silica that increase with the increase of Si/Al ratio as confirmed by XRD and IR.[1,8,27] Despite these residues, the gel appears evenly distributed yielding matrices with high homogeneity. The gel is similar to that described for fly ash-based inorganic polymer cements (IPC).[28,29]

The results of the MIP analysis of the fine pores (diameter <20 μm) are shown in Fig. 2a. Samples IP25M and IPT present the lowest cumulative pore volumes (271 and 244 $mm^3/g$ respectively) with the average pore size of 0.018 μm (18 nm) for IP25M and 0.013 μm (13 nm) for IPT. For IPMT, IP75M and IPM, the cumulative pore volume was found to be 308, 303 and 318 $mm^3/g$ respectively while the average pore size was 0.024, 0.025 and 0.031 μm. The volume fraction (%) of gel pores (pore size ≤15 nm) were $X_1 = 13.4$ for IPM; $X_2 = 39.6$ for IP75M; $X_3 = 47.4$ for IPMT; $X_4 = 40$ for IP25M; $X_5 = 93.6$ for IPT. This fine porosity include in order of size, boundary grooves, vanishing pores, grain surface features, grain and agglomerate pores. The high proportion of fine pores in an inorganic polymer has been described by Lloyd et al.[28,29] in their study on the microstructure of IPC gels. They indicated that capillary pores appear to be absent in well reacted alkali activated IPC paste and that the porosity in the IPC consists of fine, evenly distributed pores formed by the interstices of the gel particles.

In this application where insulation and not strength is the overriding factor, manual or mechanical vibration of the pastes generally used to remove air voids in IPC was avoided with the aim to improve the incorporation of additional voids into the final matrix. The spatial arrangement of these air voids and the major part of the larger-diameter pores appear in the MIP analysis with significant errors.[3,19–22,28,29] So we considered the computer micro tomography analysis to evaluate the pores with

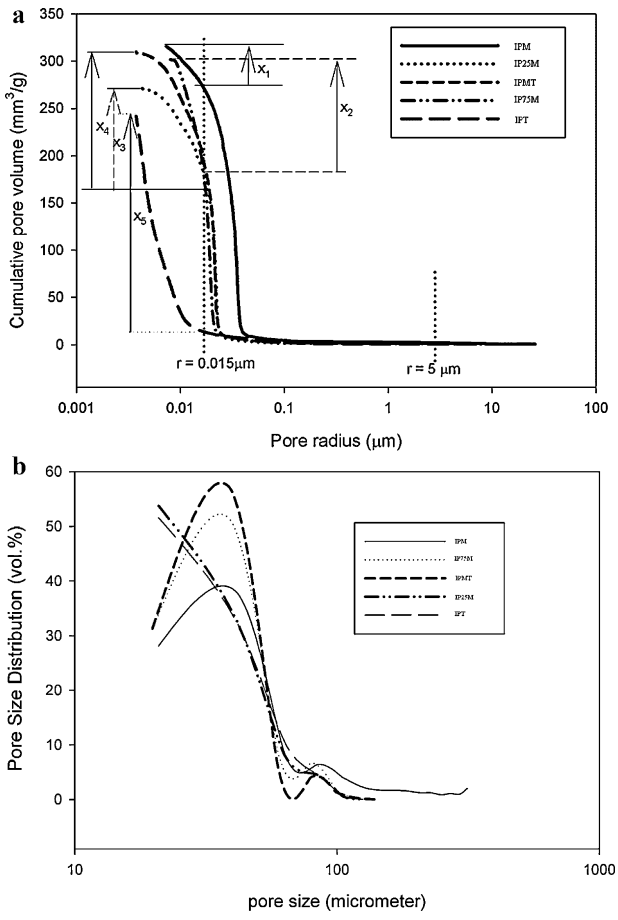


Fig. 2. (a) Pores size distribution in geopolymer compositions ($\phi < 20$ μm): volume fraction (%) of gel pores are $X_1 = 13.4$ for IPM; $X_2 = 39.6$ for IP75M; $X_3 = 47.4$ for IPMT; $X_4 = 40$ for IP25M; $X_5 = 93.6$ for IPT. (b) Pore size distribution in geopolymer compositions ($\phi > 20$ μm).

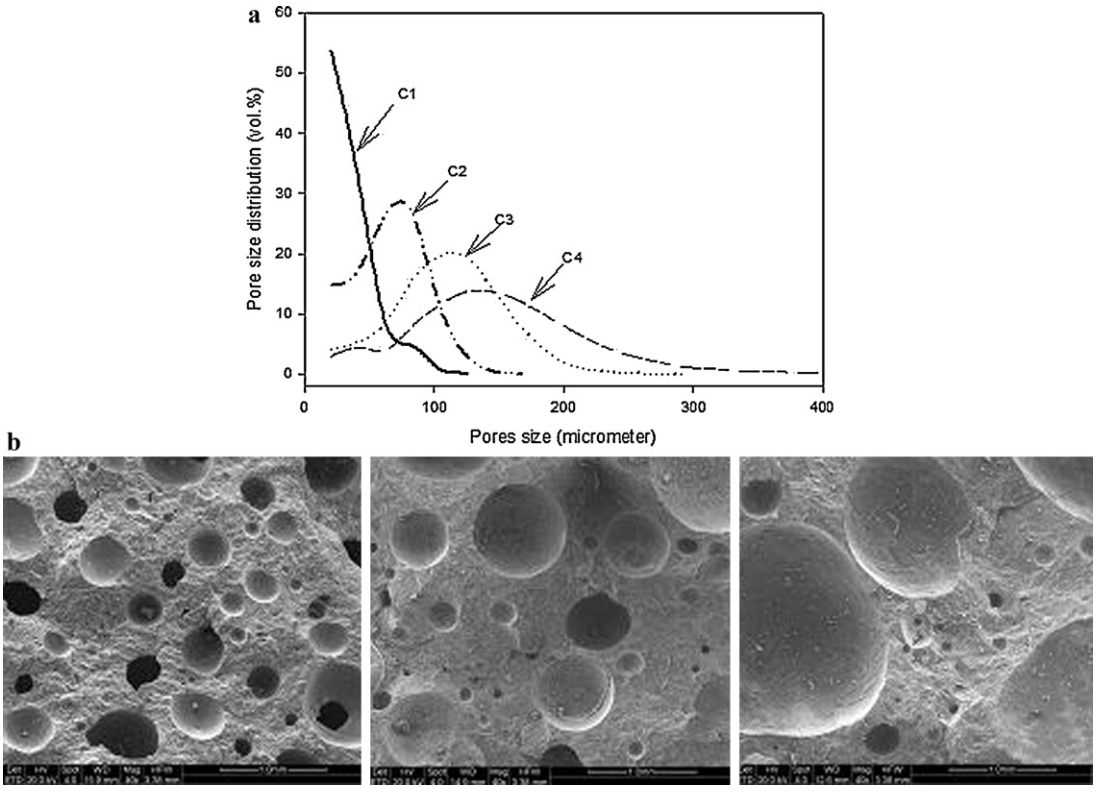


Fig. 3. (a) Variation of the pores size in porous geopolymer matrices with concentration of porous agent: lines C2, C3 and C4 for IPMT or IP25M. (b) Micrographs of porous geopolymer showing the variation of pore size with concentration of foaming agent: (left) C2, (centre) C3, (right) C4.

size ≥20 μm. As shown in Fig. 2b, the higher the alumina content (low Si/Al molar ratio), the higher was the concentration of larger-diameter pores. The samples IPMT, IP75M and IPM, with a Si/Al molar ratio ≤1.79, have larger-diameter pore size concentrated around 35, 36 and 38 μm. For the samples IP25M and IPT, the larger-diameter pore size was found to be less than 21 μm (Fig. 2b). The pore volume of larger pores which is around 3 vol.% in matrices with Si/Al <1.79 increases to 7 vol.% for IPM with Si/Al = 1.23. The porous IPC samples investigated here can be described as a semi-amorphous (gel type) matrix with high concentration of fine pores intrinsic to the parent gel together with controlled additional large pores added with pore forming agent.

The introduction of the foaming agent contributes to increasing the number and size of meso and macro pores while the solid matrix apparently maintains the same proportion of fine pores suggesting very little influence of the foaming agent in the bulk chemistry of the geopolymer matrices. A significant increase of larger-diameter pores appeared with concentration C1; as the pores in the geopolymer material remained essentially fine (nanosizes) for the lower concentration (Co). By increasing the concentration of the foaming agent (C2, C3 and C4), the cumulative pore volume of the final matrices increased and lightweight products were obtained with significant changes in the spatial distribution of pores (Fig. 3a). The volume of larger-diameter pores goes from 3 to 7 vol.% for the original geopolymers to ∼40 vol.% to highly porous ones with concentration C4 of foaming agent. From micrographs obtained with ESEM (Fig. 3b), a homogeneous distribution of meso and micro pores in the matrices can be observed.

Fig. 4a shows the pore size distribution at different Si/Al ratios for concentration C1 and Fig. 4b the average pore size (fine pores) at different foaming agent concentrations. It can be observed from Fig. 4 that the pore size distribution is directly affected by the Si/Al molar ratio, as already revealed by microtomography and MIP analyses (Fig. 2b). Higher alumina content yields a larger volume of meso and macro pores. The volume of larger-diameter pores which was generally low in the dense geopolymer compositions increases and becomes the major contribution in porous geopolymers (40 vol.%). For all compositions, round shaped pores characterize the matrices (Fig. 4). The pore development and pore size were affected with significant pore coalescence at low Si/Al ratios, while a relatively fine size of round pores characterized the high Si/Al ratios (Fig. 5a and b). When the same concentration of foaming agent is used the pore shape for the porous geopolymer is directly affected by the bulk chemical composition. Generally the average pore size in the dense regions of the porous geopolymer increases as the concentration of the foaming agent increases (Figs. 4b and 5b). When the total porosity >70 vol.%, the structures obtained were not easy to describe geometrically and samples with concentration >C4 were not considered for this study.

The behaviour of the porous geopolymers for absorbing humidity is summarized in Fig. 6. After complete curing and drying of specimens, it was observed that porous geopolymers can cumulate up to 8 wt% of humidity when stored at room

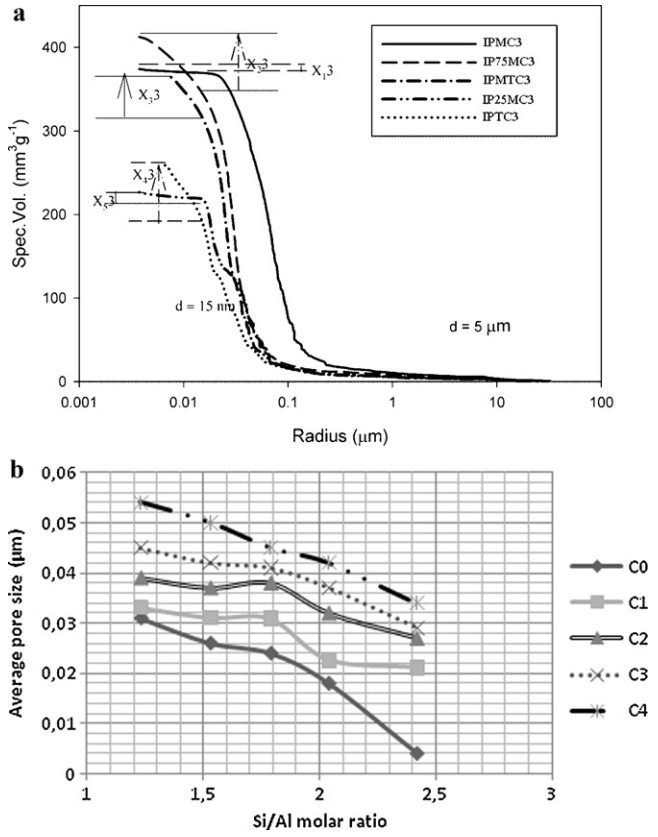


Fig. 4. (a) Pores size distribution in porous geopolymer compositions (C3; $\phi < 20\,\mu m$): volume fraction (%) of meso and macro pores are $X_1 3 = 84.06$ for IPM; $X_2 3 = 83.26$ for IP75M; $X_3 3 = 85.4$ for IPMT; $X_4 3 = 81.75$ for IP25M; $X_5 3 = 73.61$ for IPT. (b) Variation of the average pore size with the addition of the porous agent in the compact region.

temperature. After treatment at 100 °C, the time taken to resorb the original humidity was long as indicated in Fig. 6. The capacity of absorption also depends on the bulk chemical composition, as well as the nature and size of pores. It is of considerable advantage for these materials, prepared by a more environmentally friendly process, to be used as materials for surface cooling by water evaporation due to for their humidity retention capacity. Others applications linked to their insulation behaviour include energy saving in building and construction, refrigeration, thermal barriers, etc.

### 4.2. Thermal conductivity of inorganic polymer cements

The thermal conductivity values of the samples of IPC without addition of pore forming agent (Co) are $0.45\,W\,m^{-1}\,K^{-1}$ for IPM, IP75M and IPMT; $0.55\,W\,m^{-1}\,K^{-1}$ for IPT and 0.59 for IP25M with a standard deviation of $0.005\,W\,m^{-1}\,K^{-1}$ as described in our previous work.[1] The first series of samples (IPM, IP75M and IPMT) are dense geopolymer matrices with a Si/Al molar ratio <2, IP25M and IPT with Si/Al ≥2, exhibit higher density values. Based on these results, it was then suggested that the concentration of silica that is responsible for enhancing the polycondensation and as a consequence the densification, can be identified as one of the basic parameters governing the variation of the thermal conductivity of these samples. However the variation of the Si/Al ratio in these formulations also includes the variation in the amount of the residual quartz that does not transform totally during calcination of Si-rich kaolin and dissolution–polycondensation processes. Residual quartz will lead to increase of the effective thermal conductivity of IPC since the crystal exhibits thermal conductivity values in the range of 6–11 $W\,m^{-1}\,K^{-1}$ while the thermal conductivity value of amorphous silica is three to five times lower.[1,15]

With the increase of the total porosity, the effective thermal conductivity decreases as it can be observed in Fig. 7. Introducing the foaming agent in the geopolymer matrix, changes in pore size, volume fraction and spatial arrangement of pores occurred and the materials is light in weight. However, the solid phase remained continuous with connected particles despite significant fine porosity.

At 40 vol.% of pores, the thermal conductivity decreases, for all the samples, under $0.403\,W\,m^{-1}\,K^{-1}$ apart for sample IPT. A further increase in cumulative pore volume tends to reduce the difference in thermal conductivity for the respective samples. It can be noted that for higher cumulative pore volume, the impact of bulk composition on the effective thermal conductivity is reduced (Fig. 7). Mathematically, the variation of the effective thermal conductivity can be described as a function of the total porosity ($x$) with the equation (Eq. (14)) below:

$$y = bx^{-a} \tag{14}$$

with a being 1.63, 1.56, 1.45, 1.29 and 1.26; $b$ being 155, 123, 67, 38 and 34 respectively for IP25M, IPT, IPM, IP75M and IPMT. The squared correlation coefficient $R^2$ is 0.99, 0.95, 0.98, 0.98 and 0.98 respectively. Although we did not consider Schulz's model in the list of models used as reference for many reasons, Eq. (14) can be compared to the equation of Schulz's model (Eq. (15)).[30]

$$\frac{\lambda_{eff}}{\lambda_s} = (1 - v_p)\frac{1 - \cos^2\alpha}{1 - F} + \frac{\cos^2\alpha}{2F} \tag{15}$$

Schulz's model takes into account the form and the orientation of the pores and might be considered as potential analytical model for the description of porous geopolymers. Hence by introducing controlled porosity in the geopolymer formulation, the resultant material yields low values of effective thermal conductivity of interest for thermal insulation.

### 4.3. Analysis of the coefficient of conductivity $\lambda_{eff}/\lambda_s$ of the porous geopolymers with the existing models

To predict the variation of the effective thermal conductivity as function of cumulative pore volume, the analytical models developed by Maxwell–Eucken,[13] Hashin–Shtrikman (HB),[2] and Landauer[15] were used considering the cement/bound nature of the inorganic polymer cements. Analytical calculations require knowledge of the thermal conductivity of the solid phase ($\lambda_s$). The values for each sample were obtained from the extrapolation to zero percent of porosity of the experimental measurements made on the specimens without addition of pore

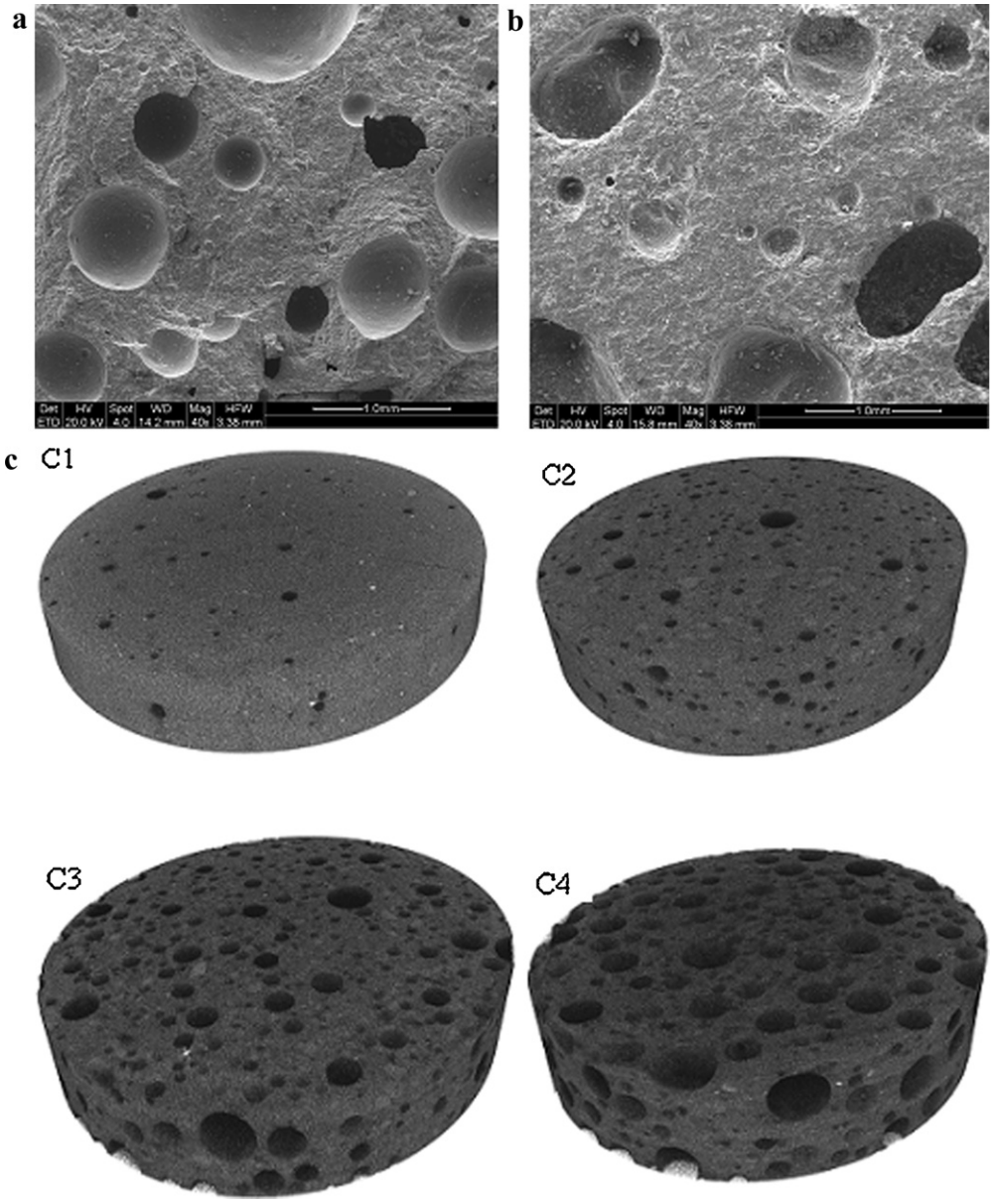


Fig. 5. (a) Pores shape in low (a) and high (b) Si/Al porous geopolymers matrices. (b) Microtomographs of the sample 25M with C1, C2, C3 and C4 concentrations.

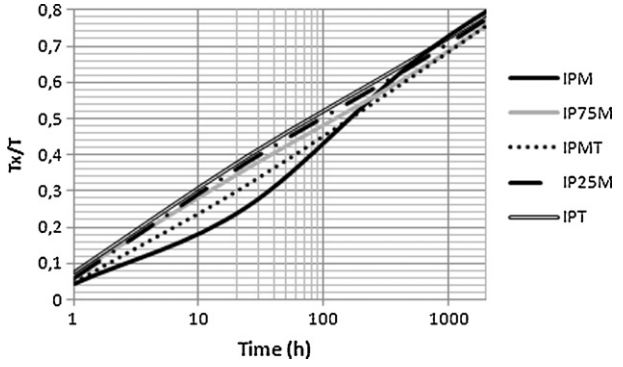


Fig. 6. Variation of $T_x/T$ (percent of humidity absorbed after exposure to ambient air/total humidity at 100 °C) with time (h).

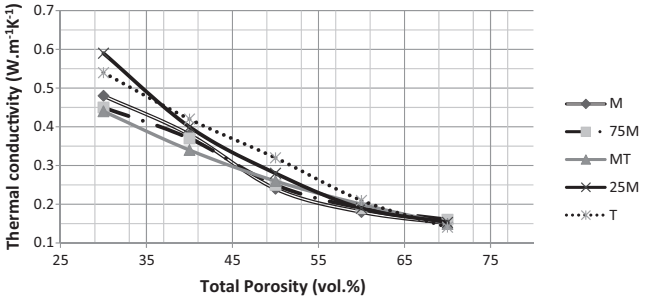


Fig. 7. Variation of the thermal conductivity ($W\,m^{-1}\,K^{-1}$) of the porous geopolymers with total porosity (vol.%).

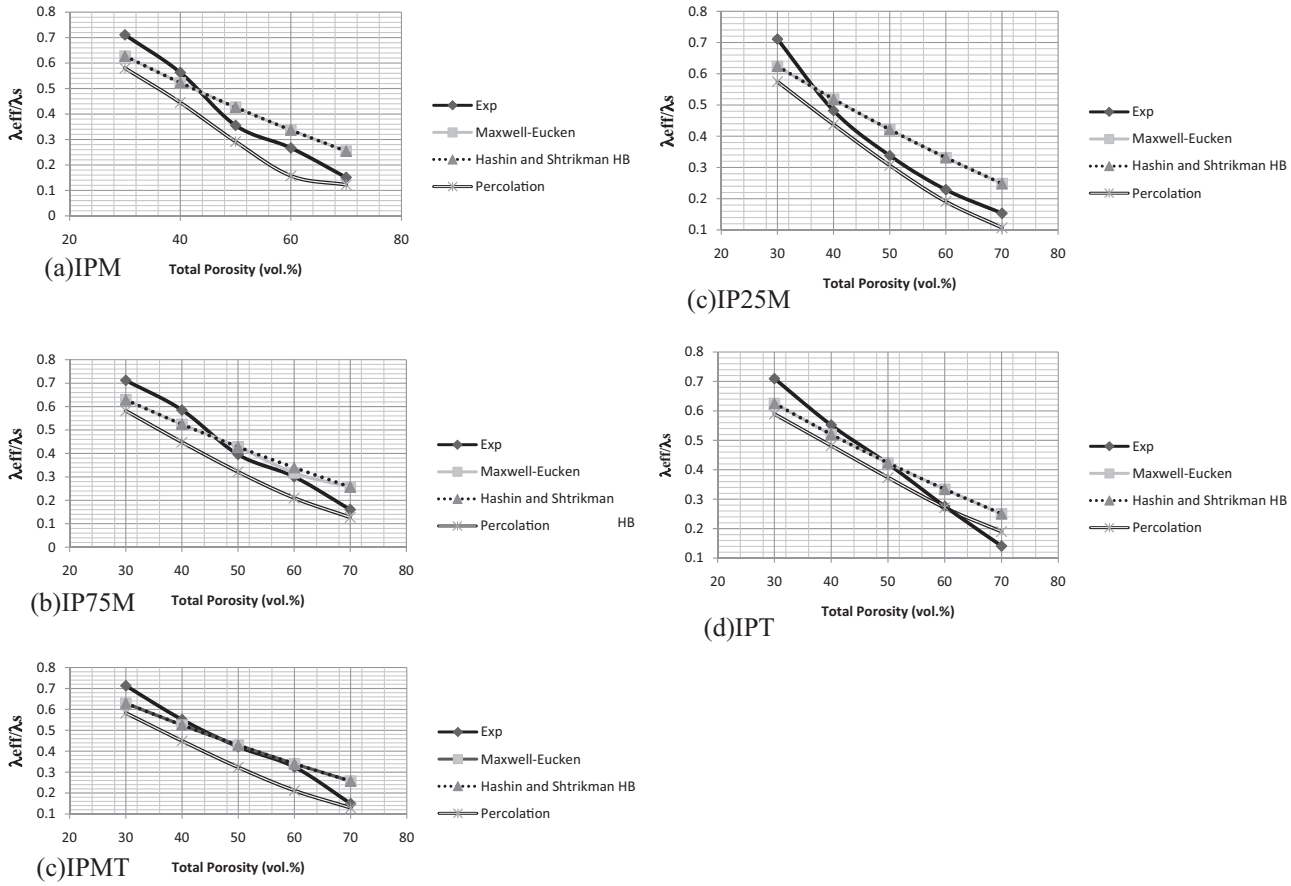


Fig. 8. Variation of the conductivity coefficient ($\lambda_{eff}/\lambda_s$) with the total porosity (vol.%) applying models of effective thermal conductivity: (a) IPM; (b) IP75M; (c) IPMT; (d) IP25M; (e) IPT.

forming agent. The values of thermal conductivity of the solid phase were 0.68, 0.64, 0.62, 0.83 and 0.77 W m$^{-1}$ K$^{-1}$ for IPM, IP75M, IPMT, IP25M and IPT. It can be noted that the formulations IPT and IP25M, which contain more residual quartz exhibit the highest extrapolated thermal conductivity at zero pore volume fraction: 0.77 and 0.83 W m$^{-1}$ K$^{-1}$ respectively. These results are in agreement with the effect of the residual crystallised phases on the thermal conductivity discussed in the previous paragraphs.

In Fig. 8a–e, the variation of the $\lambda_{eff}/\lambda_s$ coefficient with the porosity for each sample is compared with the analytical models considered. For the samples IPM (Fig. 8a), IP75M (Fig. 8b) and IPT (Fig. 8e), the values of the coefficient of conductivity ($\lambda_{eff}/\lambda_s$) remained higher than that of any of the analytical models considered for 30 and 40 vol.% of porosity.

The value of 0.71 W m$^{-1}$ K$^{-1}$ at 30 vol.% for IPM, IP75M and IPT correspond to that of Hashin–Shtrikman (HB) and Maxwell–Eucken with an accuracy of ∼0.1 W m$^{-1}$ K$^{-1}$. At 40 vol.% of porosity, the value 0.56 W m$^{-1}$ K$^{-1}$ for IPM and IP75M correspond to that of Hashin–Shtrikman (HB) and Maxwell–Eucken with 0.05 W m$^{-1}$ K$^{-1}$ of accuracy. These deviations are reasonably high making experimental results far from being described by the considered models. However, predicted results are to some extent being influenced by the sensitivity of the extrapolation of the experimental values not discussed here.

The values of 0.55, 0.42 and 0.32 W m$^{-1}$ K$^{-1}$ of IPMT for porosity of 40, 50 and 60 vol.% are close to the Maxwell–Eucken and Hashin–Shtrikman (HB) and those of 0.48, 0.34, 0.33 and 0.24 W m$^{-1}$ K$^{-1}$ of 25M are close to the percolation model. Above 40 vol.% of cumulative pore volume, the analytical models used in this work appeared as minimum and the maximum for the values of $\lambda_{eff}/\lambda_s$ of the porous geopolymers (Fig. 8). The only exception is for IPT which presented a value lower than that of any analytical model at 70 vol.%. As indicated above, the increase in cumulative pore volume reduces the influence of the bulk composition on the variation of the effective thermal conductivity.

The matrices of IPMT and IP25M without pore forming agent were dense and homogeneous resulting from a relative stable equilibrium in oligomers (Al and Si) formed and the development of more Si-polysialates, polycondensation with increases in cross linking between grains and polysialates particles.[4,5,8] Fine pores and a high degree of connectivity of polysialates and particles characterized these two matrices (Figs. 2 and 4).[8] The cross linking and better densification correlated with the pore size and pore distribution of the final matrix of geopolymer.[3–5,8] Within the framework, the porous system is viewed as a periodic three-dimensional structure with voids, in which an elementary cell of simple geometry can be, isolated (Fig. 5). The low amount of pore coalescence, the homogeneity of the solid matrix of IP25M and IPMT enable the resultant composites to behave as

a continuous solid with porosity as a second dispersed phase. The final product acts as two phases as described in many of the models considered.[2,13,14,31]

## 5. Discussion and conclusion

One of the most important advantages of the inorganic polymer cements is the simplicity of the synthetic process which allows modifying the pore size, the total porosity and potentially the pore spatial arrangement during processing. The thermal physical properties can then be monitored by controlling the cumulative pore volume, dispersed phase (air, gas, etc.) and then lowering of the effective thermal conductivity. The final material results with improved insulating behaviour: insulating material with thermal conductivity of 0.15 $W\,m^{-1}\,K^{-1}$ was achieved. A good thermal insulating material for structural application must also have adequate mechanical properties. So we concentrated our investigations on a range of the geopolymer formulations for which the behaviour under mechanical and chemical environmental stresses have been tailored.[4,8,27–29,32] From our investigations, the use of geopolymer pastes as precursors for the development of porous insulating materials required a homogeneous matrix. In fact, the results demonstrated that gel compositions with better mechanical properties and chemical stability are those where homogeneously dispersed fine pores can be easily introduced.

Formulations IPM and IP75M with Si/Al <1.79 exhibited a high volume of larger diameter-pores and a relative degree of inhomogeneity. Formulations IPMT and IP25M developed high homogeneity with greater proportion of the cross-section with respect to the other formulations as they have Si/Al ratios of 1.79 and 2.07 respectively. Their pores were concentrated in the range size of 2–25 nm. Duxson et al.[4] obtained similar findings for the metakaolin-based geopolymers with Si/Al $\geq$1.65 and concluded that the increase in gel volume for a greater cross-section support the high compression loads and explain the increase of Young's modulus. They described the homogenous samples with a high degree of cross-section and fine pores (diameter between 3.9 and 24 nm). Lloyd et al.[28,29] described IPC made from fly ash as comprised of colloidalized, globular units closely bonded together at their surfaces with pore size concentrated between 2 and 30 nm. These classes of pores were also identified by Kriven et al.[3] while describing the microstructure of fully reacted regions of metakaolin-based geopolymers. Duxson et al.[4] used the same technique (MIP) as in this work, Lloyd et al.[28,29] used nitrogen sorption and Kriven et al.,[3] the SEM analysis obtaining similar results as concerning the microstructure of the gel and their porosity. So even though (i) the individual sample may possess "ink-bottle" pore shapes, as described in the literature,[17–20,26,29] so most of them can be reached by mercury only through a long percolative chain of intermediate pores of varying sizes and shapes; (ii) micro cracks, bleeding channels, etc., may occur that mitigate the accessibility effect for some small proportion of the interior sample volume, the reproducibility of results of MIP, the success of the MIP to make difference in pore size-distribution and pore volume of samples with closed chemical compositions together with the possibility to determine the threshold diameter, the intruded volume make MIP a valuable technique for the analysis of fine pores in IPC. The technique is here completed by computer micro tomography and by the ESEM observations to evaluate larger-diameter pores which is still subject of doubt in the literature.[17–20,26] Finally we compare the total porosity obtained by the techniques with those obtained with bulk and particles density to ascertain the lower degree of errors.

The mechanism of the pores development is linked to the reaction of the foaming agent with the alkaline solution (being residual solution from the geopolymerization). The reaction that is essentially exothermic produces air/$H_2$ bubbles which give rise to porosity in the processed samples. Increasing the concentration of the foaming agent leads in an increase in the amount of produced gas and consequently an increase in the pore size and total porosity. The resultant effects were the multiplication of the final volume of the geopolymer pastes and the decrease in density. Thus we managed to develop IPCs with the high pore volume (up to 70 vol.%) with additional inputs on having nanometric and micrometric sizes of pore with well designed gel compositions (IPMT, IP25M). In those samples pore coalescences and larger-diameter resulting from air voids were not significant as in low Si/Al samples.

When designing the geopolymer matrix for thermal insulation applications, it should be note that a high concentration of alumina in the initial aluminosilicate will result in the formation of an important proportion of alumina oligomers that will not participate totally in the formation of the final product.[8,26,32,33] These compositions with low Si/Al molar ratio (IPM and IP75M) were not found more suitable for the development of homogeneous porous matrices of geopolymers for insulation applications. On the other hand, when using relatively high Si/Al aluminosilicate, the amorphous nature of silica has to be verified to optimize the final porous matrix and avoid the effects of residual crystalline quartz particles. Residual crystalline particles will modify the contact surface; hence increase the thermal conductivity of the solid phase and consequently the effective thermal conductivity of the porous IPC.

Alvarez et al.[34] described the effects of pore volume and pore-size on decreasing the effective thermal conductivity as a consequence of phonon ballistic effects. Pores with nanometric size greatly enhance phonon scattering.[32] Fine pores introduced larger strain fields in materials. These randomly distributed defects induced strain fields which increase phonon scattering by clusters and effectively obstruct the cross-sectional area for heat transfer.[34–36] Authors[34,36] observed the effective thermal conductivity of porous silica to be lower than expected by porosity and bulk phonon mean free path of silicon, and small-pore membranes have smaller thermal conductivity compared to larger pore ones despite having similar porosity values. Fang and Pilon[36] described the decrease in effective thermal conductivity in the order of 2 to 3 magnitude for the same pore volume (38%) of nanoporous silica, when the diameter of pores vary from 2.61 nm to 5.21 nm. Increasing the volume of pores, the further decrease in effective thermal conductivity was pore size dependent.[34]

During the introduction of the artificial porosity, the presence of a high content of alumina oligomers[8,27,33] leads to the

development of more pore coalescence and increase in air voids. The heterogeneity, the presence of coalesced pores as well as the intensive micro cracks will affect the final results and hinder efforts of analytical description of their structures.

The MT and 25M samples that have been found to develop good strength and resistance to chemical environmental stresses,[8] present positive results in serving as pastes for highly porous materials with the fine pores homogeneously distributed in the matrix allowing their microstructure to be close to the ideal two phase structure. Two phase structure is the basic notion for considering the modelling of the porous matrix. The Maxwell–Eucken, Hashin–Shtrikman (HB) and the Percolation models were found to be the two most accurate for the analytical description of the good homogeneous porous geopolymer materials. This comprehensive understanding of the relationship between the microstructure of porous matrices and their thermo physical properties is important in view of designing environmental-friendly materials with improved insulating performance. Moreover, an ideal analytical model should take the pore size into account to allow better description-modelling of porous geopolymers.

## Acknowledgements

Bruno Ceron-Nicolat and Tobias Fey, Department of Materials Science, University of Erlangen-Nurnberg, Martensstr. 5 D-91058 Erlangen, Germany, are kindly acknowledged.

## References

1. Kamseu E, Leonelli C, Muscio A, Libbra A. CIMTEC 2010 - Symposium CK - Geopolymers and geocements: low environmental impact ceramic materials. In: *12th International Ceramics Congress*, Montacatini (FI), Italy, June 6–11. 2010.
2. Hashin Z, Shtrikman SA. Variational approach to the theory of the effective magnetic permeability of multiphase materials. *J Appl Phys* 1962;**33**: 3125.
3. Kriven WM, Bell JL, Gordon M. Microstructure and microchemistry of fully-reacted geopolymers and geopolymer matrix composites. *Ceram Trans* 2003;**153**:227–50.
4. Duxson P, Provis JL, Lukey GC, Mallicoat SW, Kriven WM, Van Deventer JSJ. Understanding the relationship between geopolymer composition, microstructure and mechanical properties. *Colloids Surf A: Physicochem Eng Aspects* 2005;**269**:47–58.
5. Duxson P, Mallicoat SW, Lukey GC, Kriven WM, Van Deventer JSJ. The effect of alkali and Si/Al ratio on the development of mechanical properties of metakaolin-based geopolymers. *Colloids Surf A: Physicochem Eng Aspects* 2007;**292**(1):8–20.
6. Rowles M, O'Connor B. Chemical optimization of the compressive strength of aluminosilicate geopolymers synthesized by sodium silicate activation of metakaolinite. *J Mater Chem* 2003;**13**:1161–5.
7. Duxson P, Grant Lucky C, van Deventer JSJ. Thermal conductivity of metakaolin geopolymers used as first approximation for determining gel interconnectivity. *Ind Eng Chem Res* 2006;**45**:7781–8.
8. Kamseu E, Leonelli C, Chinje Melo UF, Perera D, Lemougna LN. Polysialate matrixes from Al-rich and Si-rich metakaolins: polycondensation and physico-chemical properties. *Interceram* 2011;**60**(1): 25–31.
9. Collishaw PG, Evans JRG. An assessment of expressions for the apparent thermal conductivity of cellular materials. *J Mater Sci* 1994;**29**:2261–73.
10. Smith WO. The thermal conductivity of dry soil. *Soil Sci* 1942;**53**:425–59.
11. Woodside W, Messmer JM. Thermal conductivity of porous medias. *J Appl Phys* 1961;**32**(9):1688–706.
12. Johansen O. Varmeledningseve av Jordarter, PhD thesis. Trondheim, Norway: Norge tekniske hogskole; 1975.
13. Wang J, Carson JK, North MF, Cleland DJ. A new approach to modeling the effective thermal conductivity of heterogeneous materials. *Int J Heat Mass Transfer* 2006;**49**:3075–83.
14. Broadbent SR, Hammersley JM. *Proc Camb Philos Soc* 1957;**53**:629.
15. Landauer R. The electrical resistance of binary metallic mixtures. *J Appl Phys* 1952;**23**:779–84.
16. Christon M, Burns PJ, Sommerfeld RA. Quasi-steady temperature gradient metamorphism in idealized dry snow. *Heat Transfer A: Appl* 1994;**25**(3):259–78.
17. Maxwell JC. *A treatise on electricity and magnetism*. 3rd ed. New York: Dover Publications Inc; 1954 [reprinted, chapter 9].
18. Nait-Ali B, Haberko K, Vesteghem H, Absi J, Smith DS. Thermal conductivity of highly porous zirconia. *J Eur Ceram Soc* 2006;**26**:3567–74.
19. Kaufmann J. Characterization of pore space of cement-based materials by combined mercury and wood's metal intrusion. *J Am Ceram Soc* 2009;**92**:209–16.
20. Gallé C. Effect of drying on cement-based materials pore structure as identified by mercury porosimetry: a comparative study between oven, vacuum and freezing-drying. *Cem Concr Res* 2001;**31**:14677.
21. Rigby S, Fletcher R. Interfacing mercury porosimetry with nitrogen sorption. *Part Part Syst Char* 2004;**21**:138–48.
22. Diamond S. Mercury intrusion porosimetry an inappropriate method for the measurement of pore size distributions in cement-based materials. *Cem Concr Res* 2000;**30**:1517–25.
23. Lee HHD. Validity of using porosimetry to characterise the pore structure of ceramic green compacts. *J Am Ceram Soc* 1990;**78**(8):2309–15.
24. Katrin Rubner, Dirk Hoffmann. Characterization of mineral building materials by mercury-intrusion porosimetry. *Part Part Syst Char* 2006;**23**: 20–8.
25. Lu P, Lannutti JJ. X-ray computer tomography and mercury porosimetry for evaluation of the density evolution and porosity distribution. *J Am Ceram Soc* 2000;**83**(3):518–22.
26. Zhao J, Harmer MP. Effect of pore distribution on microstructure development: I. Matrix pores. *J Am Ceram Soc* 1988;**71**(2):113–20.
27. Kamseu E. Geopolymer materials as new matrices for Structural and Insulating Applications, PhD thesis. Modena: University of Modena and Reggio Emilia; 2011. p. 191.
28. Lloyd RR, Provis JL, van Deventer JSJ. Microstructure and microanalysis of inorganic polymer cements. 2: the gel binder. *J Mater Sci* 2009;**44**:620–31.
29. Lloyd RR, Provis JL, Smeaton KJ, van Deventer JSJ. Spatial distribution of pores in fly ash-based inorganic polymer gels visualized by wood's metal intrusion. *Microporous Mesoporous Mater* 2009;**126**:32–9.
30. Schulz B. Thermal conductivity of porous and high porous materials. *High Temp–High press* 1981;**13**:649–60.
31. Kirkpatrick S. Percolation and conduction. *Rev Mod Phys* 1973;**45**:574–88.
32. Weng L, Sagoe-Crentsil K. Dissolution processes, hydrolysis and condensation reactions during geopolymer synthesis: Part I-low Si/Al ratio systems. *J Mater Sci* 2007;**42**:2997–3006.
33. Davidovits J. *Geopolymer chemistry and applications*. USA: Publ. Morrisville; 2008. p. 570P.
34. Alvarez FX, Jou D, Sellitto A. Pore-size dependence of the thermal conductivity of porous silicon: a phonon hydrodynamic approach. *Appl Phys Lett* 2010;**97**:033103.
35. Song D, Chen G. Thermal conductivity of periodic microporous silicon films. *Appl Phys Lett* 2004;**84**:687.
36. Fang J, Pilon L. Scaling laws for thermal conductivity of crystalline nanoporous silicon based on molecular dynamics simulations.